Analytical Methods

Accepted Manuscript

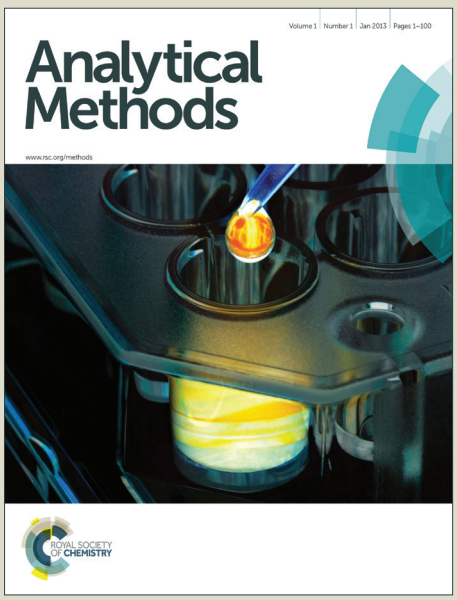

ROYAL SOCIETY OF CHEMISTRY

www.rsc.org/methods

Mapping the Reactions of Hexavalent Chromium [Cr(VI)] in Iron Nanoparticles with Spherical Aberration Corrected Scanning Transmission Electron Microscopy (Cs-STEM)

Lan Ling and Wei-xian Zhang*

Received (in XXX, XXX) Xth XXXXXXXXX 20XX, Accepted Xth XXXXXXXXX 20XX
DOI: 10.1039/b000000x

Near atomic-resolution elemental mapping on the reactions of Cr(VI) with nanoscale zero-valent iron (nZVI) is achieved by Cs-STEM integrated with EDS. Results capture for the first time detailed images that Cr diffuses across the oxide layer and accumulates primarily in the core area of nZVI, provide direct evidence on the intraparticle diffusion and reaction mechanism of Cr(VI) in a single nZVI particle, and demonstrate a unique approach for encapsulation of toxic substances.

Hexavalent chromium [Cr(VI)] is widely used for industrial applications and is an ubiquitous pollutant in the environment.[1-2] Due to its known toxic effects, concerted efforts have been made to mitigate Cr(VI) pollution.[3-5] In recent years, nZVI has been increasingly used in chromium treatment and remediation.[6-13] Our previous work showed that one gram of nZVI can remove about 0.6–0.65 grams of Cr(VI) from contaminated water, or approximately 66% of the theoretical maximum efficiency.[4,13] Moreover, nZVI is a magnetic nanomaterial, can be conveniently separated from water and soil after embedded with the targeted pollutant such as Cr.

Various mechanisms on the Cr(VI)-nZVI reactions have been proposed including aqueous phase reduction by ferrous iron [Fe(II)] and reduction by hydrogen originated from iron oxidation in water. The aqueous chemistry of Cr(VI) reduction is well known. Cr(VI) (in the form of dichromate, $Cr_2O_7^{2-}$) is a potent oxidant, reacts quickly with zero-valent iron (Fe^0), and is reduced to Cr(III) hydroxide. Meanwhile, Fe^0 is oxidized to Fe(II) and Fe(III), eventually forms complexes with the reduced Cr [$(Cr_xFe_{1-x})(OH)_3$, $Cr_xFe_{1-x}OOH$].[11-13] The ferric ion can be quickly hydrolyzed to form hydroxides [$Fe(OH)_n$], which act as flocculants and promote aggregation of nanoparticles.

Solid phase reduction by Fe^0 is generally regarded as the most important mechanism for Cr removal and treatment. Thus a fundamental question for the study of the Cr(VI)-Fe^0 reactions is the diffusion and reaction processes in the solid phase. The surface reactions, especially the reactions within the solid phase have been studied by the use of XPS, EXAFS and XRD.[13, 14] Nonetheless, these methods are statistically averaged methods that assume homogeneity across a large number of sample particles. Little information on the intraparticle reactions within individual nanopartices exists. Insights can be obtained if elemental translocation in the individual nanoparticle is directly visualized. A method with high spatial resolution and chemical sensitivity is thus desired, a technical challenge until the recent development of atomic-resolution spherical aberration corrected scanning transmission electron microscopy (Cs-STEM).[15]

In this work, a state-of-the-art Cs-STEM integrated with high-sensitive X-ray energy dispersive spectroscopy (EDS) is applied to map the reactions of dichromate ($K_2Cr_2O_7$) with individual nZVI particles. In addition to the accurate characterizations on the morphological and structural evolutions of the iron nanoparticles, a super-sensitive EDS simultaneously generates near atomic-scale details on the elemental distribution and translocations of Fe, O and Cr within a single nanoparticle. The collected data provide direct evidence on the intraparticle reactions. To our best knowledge, no systematic research has been published on this topic.

The iron nanoparticles for the STEM analysis were collected from batch reactors containing 100 mL $K_2Cr_2O_7$ solution (100 mg L^{-1} as Cr) with pre-determined doses of iron nanoparticles (e.g., 1–5 g L^{-1}). Batch reactors were sealed with screw caps and mixed on a shaker table at ambient temperature (approximately 22 ℃). The collected nZVI particles were rinsed twice with high-purity nitrogen-purged ethanol and stored in a nitrogen-purged sample vial before the STEM analysis. All reagents used (e.g., $FeCl_3$•$6H_2O$, $NaBH_4$, $K_2Cr_2O_7$) were analytical grade or better. Ultra pure deionized (DI) water was used in all solution preparations. Procedures used in the preparation and characterization of iron nanoparticles have been published elsewhere.[16]

It should be noted that the concentration of Cr(VI) used in this work is much higher than typically encountered in the environment. The instrument is capable of detecting Cr at parts per million levels or lower. However, an atomic percentage above 1% offers much better visual effect and offers minimal EDS artifact.

A Hitachi STEM (HD-2700 with cold field emission gun operated at 200 kV) was used in this work.[17] The instrument is equipped with a newly developed hexapole transfer lens spherical aberration (Cs) corrector. By correcting the spherical aberration, resolution of less than 0.105 nm can be attained in the high-angle annular dark-field (HAADF) mode. It is also fitted with the secondary electron (SE), HAADF, bright-field (BF) detectors, as well as EDS (EDAX, USA) (energy resolution < 129 eV) and EELS (Gatan, UK) spectrometers. A new image-detection chamber enables a STEM image aperture to be inserted between the BF and DF detectors. Thus, SE, BF and DF images can be obtained simultaneously under optimal optical conditions. In addition to the high EDS sensitivity, adding a Cs corrector allows a large probe current to generate into a finer electron probe and achieve high speed and high spatial resolution. [18] To minimize the effect of specimen drift, a drift-correction mode was applied during the acquisition of EDS maps. Samples for STEM analysis were prepared by allowing a single drop of a dilute ethanol-based suspension of nanoparticles to dry on lacey-carbon film supported on a 200-mesh copper TEM grid (Ted Pella, Inc.) in a N_2-filled glovebox.

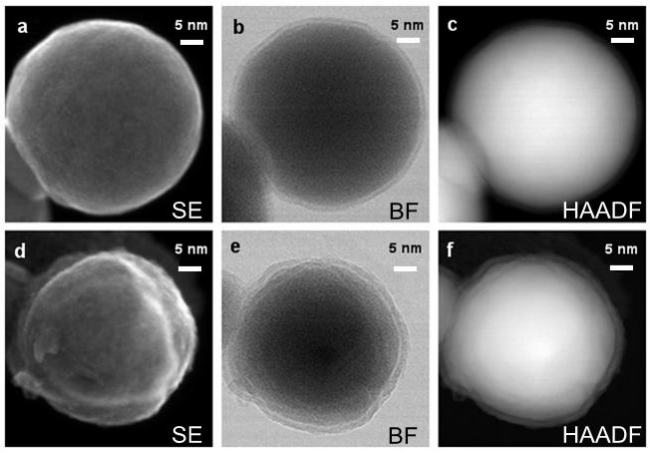

Fig. 1 STEM images of nanoscale zero-valent iron (nZVI): (a) to (c) are fresh nZVI, (d) to (f) are after 24 h reactions with 100 mg L^{-1} Cr(VI). (a) and (d) are SE images, (b) and (e) BF images, (c) and (f) HAADF images.

Figure 1 shows the structural and morphological characteristics of nZVI before (a to c) and after (d to f) reactions with 100 mg L^{-1} Cr(VI) and clearly demonstrates the reaction impacts on the iron nanoparticles. The SE, BF and HAADF images were acquired simultaneously from the same particle. A fresh nZVI particle (Fig. 1a) is spherical and typically 40–100 nm in the size as reported previously.[13] More images of nZVI are provided in the Electronic Supplementary Information (ESI, Fig. S1).

By SE imaging (Fig.1a and 1d), topographical characteristics of nZVI surface can be captured. Secondary electrons are the electrons ejected by inelastic scattering of the beam electrons from the K-shell of the specimen atoms within a few nanometers of the sample surface. Steep surfaces and edges tend to be brighter than flat surfaces, yielding images with a well-defined, three-dimensional appearance. SE image resolution less than 0.15 nm is achieved with the Hitachi HD-2700.[17]

After reactions with Cr(VI), the spherical shape of nZVI nanoparticles is distorted to some extent with irregular grain boundaries and bumpy surfaces, and covered with newly formed deposits on the surface (Fig. 1d). The individual particles are slightly smaller, but sizes of the particle aggregates are significantly larger with progressive aggregation (Fig. S1d ESI). Significant changes are also observed at the particle-particle interactions with much larger (e.g., microscale) aggregates glued together by the iron hydroxides (Fig. S1 ESI). The surface and morphological characteristics of nZVI change as a result from the progress of iron ionization, dissolution and iron hydroxide precipitation.[11,12] Dichromate as a strong oxidizing agent reacts quickly with Fe^0, and is reduced to Cr(III) hydroxide. Meanwhile, nZVI is oxidized to Fe(II) and Fe(III), eventually forms complexes with the reduced Cr.

HAADF imaging is a method of mapping by detecting the electrons scattered, predominantly elastically, through high angles. The incoherently high-angle Rutherford-scattered electrons are highly sensitive to variations in the atomic number of atoms in the sample (i.e., the Z-contrast image), with a minimum dependence on specimen thickness and microscope defocus.[19, 20] Regions of the nanoparticle with greater average through-thickness atomic number appear brighter in the HAADF image.

For Cr(VI) reactions in Fe nanoparticles (atomic numbers: Fe=26, O=8, Cr=24), Fe thus appears brighter in a HAADF image of the same thickness. As shown in Fig. 1c, the HAADF image of a clean nZVI consists of a bright core, corresponding to the metallic iron (Fe^0), and a shell of lower intensity (a mixture of Fe and O). After reactions with Cr(VI), the spent nZVI particle is nearly spherical but somewhat distorted with irregular grain boundary(Fig. 1f), individual particles still preserve the core-shell structure but with increased shell thickness. The oxide shell is partly deformed and the Fe^0 area close to the shell layer exhibits less contrast than the core (Fig. 1e), and it also shows new characteristics of multi-layers or rings in the particle (Fig. 1f). All the changes result from the surface damage during Cr reduction and Fe ionization and dissolution. At the same time, the BF images (Fig.1b and 1e) provide different but complementary view of the nanoparticles, and further support the conclusions reached on the basis of the HAADF images.[21] The above observations can be deduced based upon the chemistry of the Cr(VI)-Fe^0 reactions. The HAADF images furnish information on the size, shape, composition, related materials chemistry, and how they change with processing conditions. Thus the method is ideal for studying surface reactions.

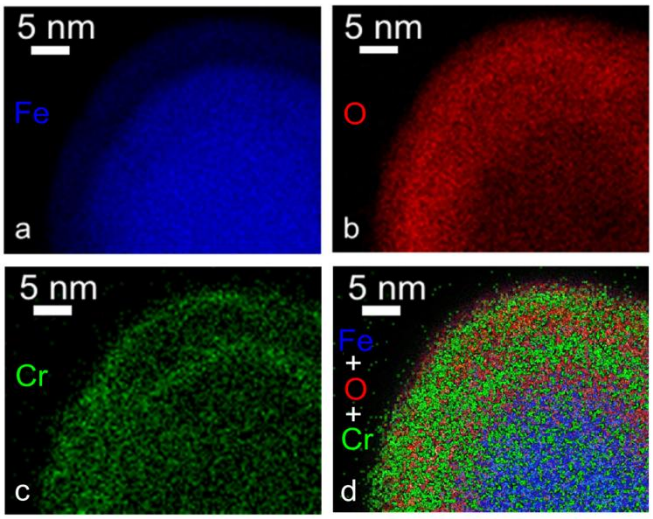

Fig. 2 STEM-EDS elemental mapping of nZVI reactions with Cr(VI): (a) Fe, (b) O, (c) Cr, and (d) Fe + O + Cr overlay.

The structure and morphology of nZVI can be interpreted more fully when considered in conjunction with their corresponding STEM-EDS elemental mapping. Fig. 2 provides STEM-EDS elemental mapping of Fe(Kα), Cr(Kα), O(Kα) and corresponding color overlays of the spent iron nanoparticle in Fig. 1d. Additional data are also available in ESI (Fig. S2). The iron mapping (Fig. 2a) shows the footprint of iron, whose surface layer appears dimmer, thus has less Fe, consistent with the core-shell structure shown in Fig. 1e and 1f. The oxygen distribution shows wide-ranging oxygen presence with the image covered extensively with oxygen (Fig. 2b). It is sparse in the core area while dense in the outer surface area, suggesting extensive oxidization in the outer shell. Our previous measurements on the spent nZVI with temperature programmed reduction (TPR) and mass spectrometer (MS) showed that Fe^0 was extensively oxidized under similar reaction conditions.[22] The Cr mapping on the other hand shows two distinctive rings of Cr in the expanded shell region and that Cr clearly reach the center of the particle (Fig. 2c and 2e), consistent with HAADF image.

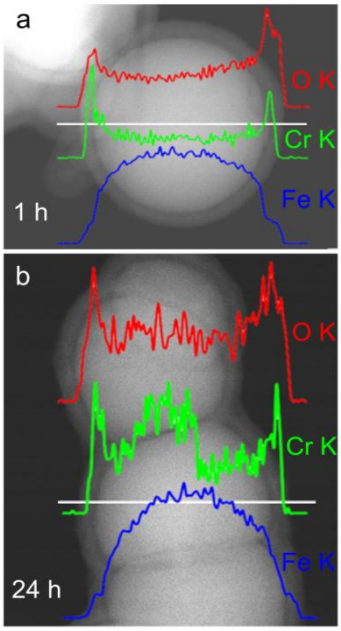

Fig. 3 Representative STEM-EDS line scan profiles of nZVI reacted with 100 mg L^{-1} Cr(VI) for 1 h (a) and 24 h (b).

With the STEM-EDS line profiles (Fig. 3), additional information on the intraparticle distribution and mass transfer of Cr during the reactions was acquired by comparing the samples after 1 h and 24 h reactions. The bell-shape iron profile after 1 h reactions (Fig. 3a) show steep decline near the particle surface due to Fe ionization and dissolution. Moreover, more decay (Fig. 3b) near the particle surface after 24 h reactions may result from further Fe ionization and dissolution. After reactions with dichromate for 1 h, Cr and O diffuse through the oxide shell and accumulate close to the iron oxide-Fe^0 interface (Fig. 3a). After 24 h reactions, Cr and O expand significantly into the interior (Fig. 3b). The area of iron oxidation is much more extensive than that of the spent nZVI for 1 h reactions, with Cr and O entrenched deeper into the particle. As proved by the Cr line profile (Fig. 3b), the most favored location for Cr is at the center of the particle where the Cr content is clearly increased from 1 h to 24 h experimental time frame (Fig. 3b). Considering the high removal rate with over 98% of the aqueous Cr(VI) removed from water in less than 30 seconds, [13] results showed in Fig.3 are not from surface precipitation, but from Cr diffusion and reduction in the core area of the nanoparticle.

The EDS mapping clearly reveals the center of nZVI as the most active area for the Cr(VI)-Fe reactions. The inner ring of Cr (Fig. 2c), which is close to the iron-rich core with highest concentration of Fe^0, appears to be the front at which the direct reduction by Fe^0 occurs. Previous work suggests that the outer ring, at the iron oxide-metallic iron interface is mostly Cr(VI) from the solution while the inner ring is the reduced form of Cr(III) [$Fe_xCr_y(OH)_3$].[13] During the reactions, Fe^0 is oxidized to Fe(II), which diffuses outward and enters the solution. Meanwhile Cr and O transfer in opposite direction. In short, the STEM-EDS mapping illustrates the characteristics of intraparticle diffusion and reactions of Cr(VI) in nZVI.

The observed distribution pattern of Cr within nZVI can be interpreted based on the nanostructure of nZVI, which contains two distinct Fe material domains (metallic and oxide iron).The iron oxide/hydroxide layer provides abundant reactive sites for coordinative reactions [i.e., sorption of Cr(VI)] while the metallic core possesses the reducing power to drive pollutants such as Cr(VI) inward, be reduced and embedded in core area instead of being retained simply as reversible surface-bound species (i.e., sorption). In the presence of excessive Fe^0, the reduced Cr is stable with minimal potential for reoxidation and dissolution. As such, nZVI exhibits much higher contaminant removal capacities (per unit of iron mass) than iron oxides and produces more stable end products.

By capturing the structural changes and elemental distributions at atomic resolution, the STEM-EDS technique thus provides direct evidence on the diffusion-reaction mechanisms in the solid phase. It appears to be a powerful tool for studying reactions in solid phase, particularly for mapping inorganic contaminants in the environmental media, and has considerable potential for studying ultrafine structural and compositional transformation induced by chemical and biological reactions in the environmental media (e.g., air, soil and water).

We acknowledge the financial support from the National Natural Science Foundation of China (NSFC Grant 21277102, 21307094), and the Science and Technology Commission of Shanghai (Grant 11JC1412600). The authors thank Hitachi High-Technologies Corporation for the use of HD-2700 STEM at its Mito (Japan) laboratory.

Notes and references

Address, State Key Laboratory for Pollution Control, College of Environmental Science and Engineering, Tongji University,1239 Siping Road, Shanghai, P.R. China. *Fax*: +86-21-65985885, *Tel*: +86-21-65982684; *E-mail*: zhangwx@tongji.edu.cn (Wei-xian Zhang).

Electronic Supplementary Information (ESI) available. Additional STEM images of nZVI after reactions with dichromate. STEM-EDS elemental maps of Fe, O, Cr of a whole nZVI particle are provided. See DOI:

1 D. E. Kimbrough, Y. Cohen, A. M. Winer, L. Creelman, M. Clayton, *Crit. Rev. Env. Sci. Tec*., 1999, **29**, 1.
2 A. S. Ellis, T. M. Johnson, T. D. Bullen, *Science*, 2002, **295**, 2060.
3 G. E. Fryxell, J. Liu, T. A. Hauser, Z. M. Nie, K. F. Ferris, S. Mattigod, M. L. Gong, R. T. Hallen, *Chem. Mater*., 1999, **11**, 2148.
4 J.S. Cao, W.X. Zhang. *J. Hazard. Mater*., 2006,**132**, 213.
5 M. Yadav, Q. Xu, *Chem. Commun.*, 2013, **49**, 3327.
6 S. M. Ponder, J. G. Darab, T. E. Mallouk, *Environ. Sci. Technol*., 2000, **34**, 2564.
7 M. J. Alowitz, M. M. Scherer, *Environ. Sci. Technol*., 2002, **36**, 299.
8 M. L. Peterson, G. E. Brown, G. A. Parks, L. S. Carol, *Geochim.Cosmochim.Ac.*, 1997, **61**, 3399.
9 R. W. Puls, C. J. Paul, R. M. Powell, *Appl.Geochem.*, 1999, **14**, 989.
10 P. Bhunia, G. Kim, C. Baik, H. Lee, *Chem. Commun*., 2012, **48**, 9888.
11 V. António, F. António, G. Fernanda, *Langmuir*, 2010, **26**, 11980.
12 N. Melitas, O. Chuffe-Moscoso, J. Farrell, *Environ. Sci. Technol.*, 2001, **35**, 3948.
13 X. Q. Li, J. S. Cao, W. X. Zhang, *Ind. Eng. Chem. Res*., 2008, **47**, 2131.
14 B. A. Manning, J. R. Kiser, H. Kwon, S. R. Kanel, *Environ. Sci. Technol*., 2007, **41**, 586.
15 P. E. Baston, N. Dellby, O. L. Krivanek, *Nature*, 2002, **418**, 617.
16 C. Wang, W. X. Zhang, *Environ. Sci. Technol*., 1997, **31**, 2154.
17 Y. Zhu, H. Inada, K. Nakamura, J. Wall, *Nat. Mater*., 2009, **8**, 808.
18 A. A. Herzing, M. Watanabe, J. K. Edwards, M. Conte, Z. R. Tang, G. J. Hutchings, C. J. Kiely, *Faraday Discuss*, 2008, **138**, 337.
19 S. J. Pennycook, L.A. Boatner, *Nature*, 1988, **336**,565.
20 E. P. W. Ward, I. Arslan, P. A. Midgley, A. Blelochb, J. M. Thomas, *Chem. Commun.*, 2005, 5805.
21 J. M. Thomas, P. A. Midgley, *Chem. Commun.*,2004,1253.
22 J. S. Cao, X. Q.Li, J. Tavakoli, W. X. Zhang, *Environ. Sci. Technol.*, 2008, **42**, 3780.

Mapping the Reactions of Hexavalent Chromium [Cr(VI)] in Iron Nanoparticles with Spherical Aberration Corrected Scanning Transmission Electron Microscopy (Cs-STEM)

Lan Ling and Wei-xian Zhang*

Institute for Environmental Chemistry

State Key Laboratory for Pollution Control

1239 Siping Road, Shanghai, P.R. China

TOC: Mapping Cr(VI) reactions with nanoscale zero-valent iron